

## TWO-PHOTON EXCITATION OF HYDROGEN PEROXIDE AT 266 AND 193 nm: DETERMINATION OF THE ABSORPTION CROSS SECTION AND PHOTOFRAGMENT STATE DISTRIBUTION

Stefan KLEE, Karl-Heinz GERICKE, Horst GÖLZENLEUCHTER and Franz Josef COMES

*Institut für Physikalische und Theoretische Chemie der Johann Wolfgang Goethe-Universität,  
Niederurseler Hang, D-6000 Frankfurt am Main 50, FRG*

Received 14 June 1989

The sequential two-photon dissociation of hydrogen peroxide into electronically excited hydroxyl radicals has been investigated at the photolysis wavelengths of 266 and 193 nm. Using a conventional rate equation approach, the differential second-photon absorption cross section at 266 nm was determined to be  $\sigma_2 \approx 2 \times 10^{-16} \text{ cm}^2$  by a comparison of the photoinduced  $\text{OH}(A^2\Sigma^+)$  emission with the laser-induced fluorescence of simultaneously formed  $\text{OH}(X^2\Pi_1)$  under the same excitation and detection conditions. The second-photon absorption cross section at 193 nm was found to be smaller by a factor of approximately 60, in accordance with the existence of additional dark dissociation channels. The analysis of the distribution of available energy into  $\text{OH}(A)$  reveals that translational excitation must be very high and, furthermore, that there is substantially less energy left in fragment rotation than expected from results of isoenergetic one-photon dissociation. The rotational state distributions in  $v' = 0$  are found to be approximately Boltzmannian with maximum populations at  $N'_{\text{OH}} \approx 6$  (266 nm) and  $N'_{\text{OH}} \approx 9$  (193 nm). The internal energy distribution of  $\text{OH}(A)$  resembles that of  $\text{OH}(X)$  following the one-photon process at the same wavelength and half of the photon energy. Thus, a model is proposed, in which the two-photon dissociation dynamics is characterized by the evolution of the intermediate state departing from the first-photon Franck–Condon region before further absorption.

### 1. Introduction

High-power pulsed UV lasers have been used to produce electronically excited atoms and free radicals from the multiphoton dissociation of numerous molecules [1,2]. The spectroscopic and dynamic information obtained from such nonlinear optical processes can complement that obtained from single-photon transitions due to the different selection rules for both phenomena [3]. Using two-photon excitation, upper electronic molecular states can be prepared, which possess, for example, in the case of inversion-symmetric molecules the same parity as the ground state. Furthermore, doubly excited states from  $\Delta J = 2$  or  $\Delta L = 2$  transitions are allowed. The excitation of these states via ordinary single-photon absorption is strictly forbidden. Furthermore, where the absorption of one or two photons leads to the population of the same upper (repulsive) electronic state, as is allowed in molecules having lower than inversion symmetry, the interesting question arises, how

far the different excitation schemes influence the dissociation dynamics as observed in the reaction energy disposal patterns of the photofragments. Whether a dynamical distinction occurs between isoenergetic one-photon and two-photon dissociation events, depends strongly on the nature and the lifetime of the participating intermediate state in the two-photon process. Prototypically, either the first photon is resonantly absorbed populating a real intermediate state or, if such a state is absent, a virtual state is excited, where the transition probability increases with the number of near-resonant real states having the appropriate symmetry. Generally, the distinguishing feature between the different excitation mechanisms is a noticeably lower absorption probability for the non-resonant process. Simultaneous absorption of a second photon by the virtual state within a time determined by the uncertainty principle gives rise to a transition into the Franck–Condon region that is also accessible in an isoenergetic ( $E = 2h\nu$ ) one-photon process. If the evolution on the upper potential en-

ergy surface of the species excited by one- or two-photon absorption causes molecular dissociation, it is expected that the dynamically equivalent photofragmentation pathways will lead to equivalent final state distributions. For example, this had been experimentally observed in recent studies of the photodissociation of  $\text{H}_2\text{O}$  and  $\text{D}_2\text{O}$  in the second continuum [4].

Otherwise, if the intermediate state is real, the sequential absorption of both photons is separated by a time delay during which evolution of the intermediate state occurs. Then the excitation to the final (repulsive) state probes a different region of the upper electronic surface than the isoenergetic one-photon process. Therefore, the dissociation pathways may diverge and the extent of the differences which arise in the fragment energy disposal depends on the time delay between the absorbed photons that is limited by the lifetime of the intermediate state. The first example of such a photolysis process was found in  $\text{NO}_2$ , where final state distributions for ultraviolet single-photon dissociation were discovered to be substantially different from those following isoenergetic visible two-photon dissociation [5]. Two-photon dissociation near 450 nm yielded  $\text{NO}(X^2\Pi)$  product radicals mainly in  $v''=0$  and 1, while 225 nm one-photon photolysis produced a  $\text{NO}$  vibrational distribution inverted in  $v''=2$ . To interpret the two-photon dissociation dynamics, a model was suggested where absorption of the first photon projected the ground state onto a dense system of vibronic intermediate states arising from at least three electronic states. The high density of electronic configurations at the intermediate level was responsible for substantial intramolecular energy redistribution.

A theoretical study of time delayed two-photon processes has been performed by Cribb and Brickmann [6]. They calculated the semiclassical probability for a transition from the vibrational ground state of the ground electronic surface to an electronically excited vibronic state via a repulsive real intermediate state as a function of different potential parameters and of the second-photon arrival time distribution. The maximum transition probability was observed to shift with the mean delay time between the two photons and to depend on the wave packet momentum gained during the propagation time. The effects become more evident with increasing dis-

placement between ground and excited surfaces.

This report describes a second molecular example, hydrogen peroxide, where the photofragmentation pathways are dynamically distinct for one-photon and isoenergetic two-photon dissociation. Photoinduced emission due to two-photon dissociation of  $\text{H}_2\text{O}_2$  has been observed following irradiation at 193 nm [7,8]. Since the upper electronic state potential of  $\text{H}_2\text{O}_2$  are sufficiently well known from experimental [9–11] and theoretical [12–14] work, a sequential excitation mechanism can be rationalized as shown in fig. 1. The first UV photon carries the molecule from the ground state ( $\tilde{X}^1A$ ) into an intermediate state, which can be identified as one of the two low-lying singlet states,  $\tilde{A}^1A$  and  $\tilde{B}^1B$ , that correlate with two OH radicals in their electronic ground state ( $X^2\Pi_1$ ). After a time delay  $\tau$ , absorption of the second photon induces a transition to a high-lying dissociative state that decays into  $\text{OH}(A^2\Sigma^+) + \text{OH}(X^2\Pi_1)$ . The  $\tilde{E}^1A$  and  $\tilde{F}^1B$  states are energetically accessible<sup>#1</sup>. They

<sup>#1</sup> The alphabetical order of the electronically excited molecular states of hydrogen peroxide considers the OH-dissociative state that has been recently observed by Gerlach-Meyer et al. [15] and calculated ab initio by Reinsch. [13].

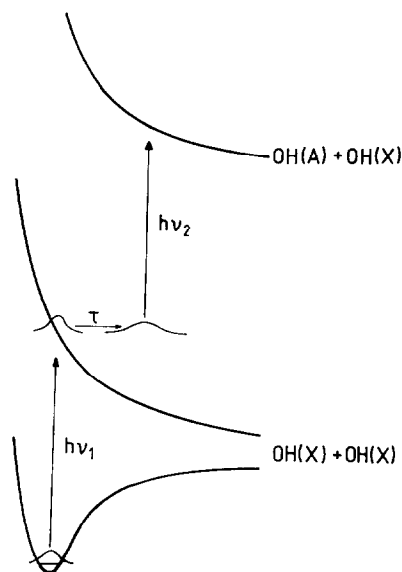


Fig. 1. Schematic illustration of the sequential two-photon excitation process in hydrogen peroxide ( $\tilde{X}^1A$ ) involving the repulsive intermediate ( $\tilde{A}^1A$  or  $\tilde{B}^1B$ ) and the final molecular state ( $\tilde{E}^1A$  and/or  $\tilde{F}^1B$ ).

are also held responsible for OH(A) generation following VUV single-photon absorption [11].

In the present study, we investigated the energy distributions of OH(A<sup>2</sup>Σ<sup>+</sup>) produced by the resonant two-photon excitation of H<sub>2</sub>O<sub>2</sub> at 266 nm and completed earlier studies of the nonlinear photodissociation of H<sub>2</sub>O<sub>2</sub> and D<sub>2</sub>O<sub>2</sub> at 193 nm [8]. The final state distributions from the two-photon processes are compared with those from single-photon excitation at various wavelengths in the UV [9,10] and VUV [11,16]. Furthermore, single-photon measurements at 266 and 157 nm were carried out for direct comparison of excitation rates. Conventional rate equations for sequential absorption lead to a calculation of the differential second-photon absorption cross section for OH(A) production following two-photon excitation of hydrogen peroxide.

## 2. Experimental

In this experiment photoinduced emission was investigated following H<sub>2</sub>O<sub>2</sub> (D<sub>2</sub>O<sub>2</sub>) excitation by either a quadrupled Nd:YAG laser (Quanta Ray, DCR-1A) operating at 266 nm or an ArF excimer laser (Lambda Physik, EMG 201 MSC) at 193 nm. The beam of the pulsed laser was focused into an aluminum cell by a 300 mm focal length quartz lens providing a power density of up to 1 GW cm<sup>-2</sup> in the focal region. The optical and electronical detection system was similar to that used in our earlier studies on OH(A<sup>2</sup>Σ<sup>+</sup>) [11]. In order to measure nascent emission spectra, fluorescence from the A<sup>2</sup>Σ<sup>+</sup>-X<sup>2</sup>Π<sub>i</sub> transition was collected, dispersed by a 0.5 m monochromator (Minuteman) and the spectrally resolved emission was detected by an optical multichannel analyzer (OSMA, Physical Instruments). The slits were oriented parallel to the laser beam axis to view exclusively emission from the double cone focal region. The resolving power of the detection system was adjustable to maximal  $\lambda/\Delta\lambda=3\times 10^4$  (grating 3600 grooves/mm, slit width 20 μm). Integration time was up to 12 min (7200 laser shots at 10 Hz) to improve the signal-to-noise ratio.

For the comparison of excitation rates in the 157 nm one-photon and 193 nm two-photon processes a grating of lower resolution (600 grooves/mm) was used to simultaneously detect the total fluorescence

between 280 and 320 nm from the (1, 0), (2, 1), (0, 0), (1, 1) and (2, 2) vibrational bands. In the single-photon experiment the setup remained unchanged, except that the excimer laser was operated with low power density ( $\approx 5$  MW cm<sup>-2</sup>) on the F<sub>2</sub> line. In this case the light path was flooded with dry nitrogen gas to avoid absorption of the VUV radiation by ambient oxygen.

At 266 nm the comparison of signal levels following two-photon-induced emission versus laser-induced fluorescence (LIF) following single-photon dissociation under the same excitation and detection conditions was achieved in a standard LIF apparatus, which has been described previously in detail [9]. Here the undispersed total emission from the two-photon dissociation was detected by a photomultiplier tube (Valvo, XP2254B, 2.8 kV) preceded by a set of imaging optics and an interference filter (310 ± 10 nm). The PMT signal was registered by a digital storage oscilloscope (LeCroy, 9450), averaged over 100 shots and subsequently integrated. Similarly the LIF signal from a single rotational line of OH(X<sup>2</sup>Π<sub>i</sub>) was detected through the same optical system following broad band resonant excitation ( $\Delta\nu_1=0.4$  cm<sup>-1</sup> fwhm) by the tunable radiation of a frequency doubled dye laser (Lambda Physik, FL 2002 E). Pump and probe beams were mutually orthogonal and the time delay between the two was 20 ns.

H<sub>2</sub>O<sub>2</sub> and D<sub>2</sub>O<sub>2</sub>, respectively, were rapidly pumped through the photolysis cell at pressures in the range of 0.1–10 Pa. The probe gas evaporated from a liquid H<sub>2</sub>O<sub>2</sub>/H<sub>2</sub>O solution with a peroxide concentration of > 95%, as determined by its refractive index [17]. This corresponded to a vapor composition with approximately 20% water. Any influence on the OH product state distribution by singly excited H<sub>2</sub>O at the photolysis wavelengths used was ruled out, since water dissociates into electronically excited hydroxyl radicals only when photolyzed below 135 nm [18]. However, care must have been taken on account of its possible two-photon excitation [4]. Therefore, the ratio of the total photoinduced emission following successive irradiation of equal amounts of the H<sub>2</sub>O<sub>2</sub>/H<sub>2</sub>O mixture and of pure H<sub>2</sub>O at 266 nm was determined and found to be 5:2. Since water only makes up 20% of the vapor in the H<sub>2</sub>O<sub>2</sub>/H<sub>2</sub>O mixtures there would only be a 6% contribution to the total OH(A)

signal from this interference. The same applied to the 193 nm experiment [7].

Deuterium peroxide was prepared by mixing  $\text{H}_2\text{O}_2$  (90%) with an excess of  $\text{D}_2\text{O}$  and distilling the mixture to higher peroxide concentration.

### 3. Intensity dependence

For an unsaturated single-photon absorption the (possibly laser-induced) fluorescence emission has to vary linearly with the photolysis laser energy. In the present case of a two-photon process a quadratic dependence is found. The log-log plot shown in fig. 2 shows the total OH(X-A) fluorescence as a function of different laser fluences for 193 nm (squares) and 266 nm (crosses) irradiation. The slope of the straight line fitted to the experimental points is  $2.0 \pm 0.1$  at 193 nm and  $1.9 \pm 0.1$  at 266 nm, respectively, clearly demonstrating the expected power dependence for a two-photon process. At high fluences ( $>0.1 \text{ GW cm}^{-2}$ ) the quadratic dependence is observed to change into a linear one due to bleaching of the  $\text{H}_2\text{O}_2(\tilde{\text{X}}^1\text{A})$  ground state [8]. The relative displacement of the curves results primarily from the uncertainties in the determination of absolute focal power densities at 266 and 193 nm.

In principle, a quadratic power dependence can be

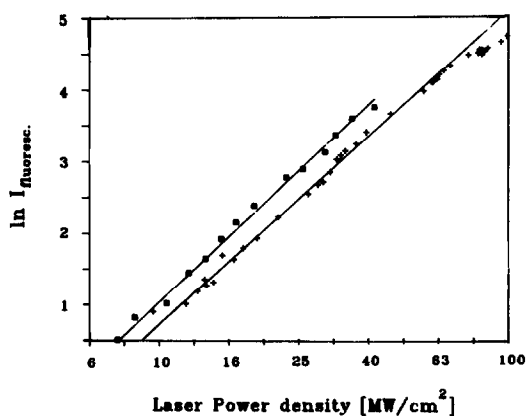


Fig. 2. Two-photon induced  $\text{OH}(\text{A}^2\Sigma^+ \rightarrow \text{X}^2\Pi_1)$  emission following excitation at 193 nm (squares) at 266 nm (crosses) as a function of the laser power density. The fitted slope in the log-log plot is  $2.0 \pm 0.1$  at 193 nm and  $1.9 \pm 0.1$  at 266 nm.

caused by secondary excitation with subsequent fluorescence emission of a product molecule formed in a single-photon process. This mechanism can be excluded in the present case because secondary absorption of photons in the far-UV by hydroxyl radicals would result in highly vibrationally excited  $\text{OH}(\text{A}^2\Sigma^+)$  radicals, which undergo extremely rapid predissociation and therefore decay non-radiatively [19].

Furthermore,  $\text{OH}(\text{A})$  could also be generated by the photolysis of hydroperoxyl radicals,  $\text{HO}_2$ , which have been observed as primary products from a minor ( $12 \pm 1\%$ )  $\text{H}_2\text{O}_2$  dissociation channel at 193 nm [15]. Since this channel is endothermic by more than  $120 \text{ kJ mol}^{-1}$  at 266 nm we do not attribute the two-photon signals to  $\text{HO}_2$  photolysis.

### 4. Second-photon absorption cross section

In principle, the exact treatment of a sequential two-photon excitation would be the solution of the time-dependent Schrödinger equation. Recently, Williams and Imre [20] have investigated single- and two-photon processes using a time-dependent formalism. In the case of cw excitation, i.e. the laser pulse length being longer than the decay time, they demonstrated that the first photon prepares the intermediate repulsive state  $|\Psi_r\rangle$ , where  $|\Psi_r\rangle$  is not a moving wave packet, but a time-independent wavefunction.

The present study of the photodissociation of hydrogen peroxide uses nanosecond laser pulses for excitation. Hence, the decay process is observed in the cw limit. The resonant two-photon dissociation of  $\text{H}_2\text{O}_2$  will be modeled by a conventional rate equation approach with sequential and competing photochemical reactions depicted schematically in fig. 3. Only irreversible first-order kinetic processes have to be considered. The experimentally observed signal  $S$ , which is proportional to the concentration of fluorescing OH radicals per unit volume,  $[\text{OH}(\text{A})]$ , is found to be (cf. eq. (4) in ref. [8]):

$$S \propto [\text{OH}(\text{A})] = [\text{H}_2\text{O}_2]_0 (\sigma_2/k_1 T) \times I [1 - \exp(-\sigma_1 I)] \quad (1)$$

$[\text{H}_2\text{O}_2]_0$  represents the initial concentration of hydrogen peroxide molecules in the ground state. The

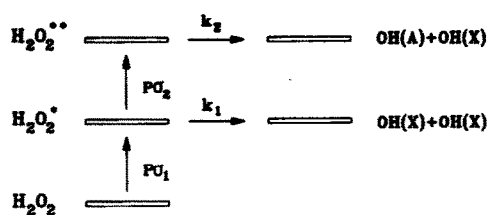


Fig. 3. Schematic representation of the rate equation approach used to model competing one-photon and two-photon excitation processes in hydrogen peroxide. The experimentally observed ratio of  $[\text{OH}(\text{X})]$  to  $[\text{OH}(\text{A})]$  depends on the relative magnitudes of pump and dissociation rates.

$\sigma_i$  ( $\text{cm}^2$ ) ( $i = 1, 2$ ) are absorption cross sections for the transitions to the intermediate state  $\text{H}_2\text{O}_2^*$  and the final state  $\text{H}_2\text{O}_2^{**}$ . The corresponding rate constants for dissociation into hydroxyl radicals are labelled by  $k_i$  ( $\text{s}^{-1}$ ). The fluence of the laser radiation  $I$  (photons  $\text{cm}^{-2}$ ) is given as the power density  $P$  (photons  $\text{cm}^{-2} \text{s}^{-1}$ ) integrated over the pulse duration  $T$  (s).

At low laser fluences ( $I < 1/\sigma_1$ ) the exponential term in eq. (1) can be replaced by  $(1 - \sigma_1 I)$  yielding the observed quadratic dependence

$$[\text{OH}(\text{A})] = [\text{H}_2\text{O}_2]_0 (\sigma_1 \sigma_2 / k_1 T) I^2. \quad (2)$$

At high fluences ( $I > 1/\sigma_1$ ) the exponential term in eq. (1) vanishes and the signal increases linearly with  $I$

$$[\text{OH}(\text{A})] = [\text{H}_2\text{O}_2]_0 (\sigma_2 / k_1 T) I. \quad (3)$$

Fig. 3 demonstrates that absorption of a second photon in the intermediate state competes with efficient dissociation into two ground state OH radicals. From very detailed LIF studies on OH(X) using sub-Doppler and polarization spectroscopy at 266 nm the first excited  $\text{H}_2\text{O}_2$  state ( $\tilde{\text{A}}^1\text{A}$ ) is known to decay within  $\tau_1 = 60$  fs [21]. Thus, the dissociation rate  $k_1 = \ln 2 / \tau_1$  greatly exceeds  $P\sigma_2$  at the given experimental laser fluences unless a very unrealistic value of  $\sigma_2 > 10^{-14} \text{ cm}^2$  is adopted.

The concentration of OH products formed in their electronic ground state,  $\text{X}^2\Pi_i$  is essentially determined by the first absorption step leading to  $\text{H}_2\text{O}_2^*$ , because the removal of  $\text{H}_2\text{O}_2^*$  by further excitation as well as the amount of OH(X) from dissociating  $\text{H}_2\text{O}_2^{**}$  is negligibly small. Because each dissociating

peroxide molecule generates two product radicals and only low laser fluences  $I < 1/\sigma_1$  are applied, the concentration of OH(X) radicals per unit volume is

$$[\text{OH}(\text{X})] = 2[\text{H}_2\text{O}_2]_0 \sigma_1 I. \quad (4)$$

The first-photon absorption cross section  $\sigma_1$  has been conventionally measured to be  $3.8 \times 10^{-20} \text{ cm}^2$  at 266 nm [22].

Dividing eq. (4) by eq. (2) yields a simple relation for the branching ratio into both dissociation channels

$$[\text{OH}(\text{X})] / [\text{OH}(\text{A})] = 2k_1 T / \sigma_2 I = 2k_1 / P\sigma_2. \quad (5)$$

In contrast to  $\sigma_1$ , the direct measurement of  $\sigma_2$  via absorption or emission detection techniques is complicated by problems of absolute determination of collection efficiencies and OH densities. We present a relative measurement of  $\sigma_2$  by comparison of signal levels obtained with two-photon excitation versus LIF detection of OH(X) radicals formed after the first-photon absorption under constant excitation and detection conditions.

The laser-induced fluorescence signal per unit volumes  $S'$  following resonant excitation of the fraction of  $\text{OH}(\text{X } ^2\Pi_i; v'' = 0, J'')$  radicals in the rotational state  $J''$  is

$$S' \propto [\text{OH}(\text{X})] P(J'') \sigma' I', \quad (6)$$

where the prime labels parameters of the LIF experiment. The population number  $P(J'')$  of a selected rotational state is well known from earlier studies [9]. The state resolved OH(X) absorption cross section  $\sigma'$  is composed of the tabulated Einstein coefficient  $B$  ( $\text{cm}^3 \text{ J}^{-1} \text{ s}^{-2}$ ) [23], the wavelength  $\lambda$  (cm), and the Doppler width  $\Delta\nu_D$  ( $\text{s}^{-1}$ ), which is assumed to coincide spectrally with the dye laser bandwidth ( $\Delta\nu_D = \Delta\nu_L$ ):

$$\sigma' = Bh / \lambda \Delta\nu_D. \quad (7)$$

Combining eqs. (5)–(7) yields the desired expression for  $\sigma_2$ :

$$\sigma_2 = \frac{S}{S'} \frac{2k_1}{P} \frac{BhP(J'')I'}{\lambda \Delta\nu_D}. \quad (8)$$

The volumes for OH radical generation and probing do not need to be treated explicitly, since they were identical because the dye laser beam overlapped the entire photolysis region. The experimental param-

ters, applicable to eq. (8), are as follows: The photolysis laser operated at an energy of 22 mJ with a 6.5 ns pulse length and had a 2 mm<sup>2</sup> cross section in the focal area. Induced OH(A) emission following irradiation of 4.0 Pa H<sub>2</sub>O<sub>2</sub> yielded a signal of 0.4 arbitrary units. Thereupon induced fluorescence following excitation of the Q<sub>1</sub>(4) transition ( $\Delta\nu_D \approx 0.40$  cm<sup>-1</sup> [21]) by the probe laser ( $I' = 5 \times 10^{-5}$  J cm<sup>-2</sup>) produced an offset of 3.9 units, thus giving  $S/S' = 0.1$ . Comparison of  $S$  with  $S'$  at the P<sub>12</sub>(1) absorption line resulted in a ratio of 0.3. Variation of the photolysis energy revealed the expected behavior where the LIF signal increased linearly with the energy in contrast to the quadratic dependence of the photoinduced emission. From the experimental signal ratios and the population numbers  $P(4) = 0.10$  and  $P(1) = 0.05$  [9], a value of  $\sigma_2 \approx 2 \times 10^{-16}$  cm<sup>2</sup> follows. This corresponds to a pumping rate into H<sub>2</sub>O<sub>2</sub><sup>\*\*</sup> of  $P\sigma_2 \approx 5 \times 10^{10}$  s<sup>-1</sup> at the typical laser intensity. The assumption that the second-photon excitation is rate-determining ( $P\sigma_2 \geq k_2$ ) sets an upper limit of  $\tau_2 \leq 15$  ps for the lifetime of H<sub>2</sub>O<sub>2</sub><sup>\*\*</sup>. Therefore it is not possible to distinguish between proposed molecular state geometries having their transition dipole oriented perpendicular ( $\tau_{\max} \approx 340$  fs) or parallel ( $\tau_{\max} \approx 100$  fs) to the O–O axis [11].

It should be pointed out that both sequential excitation steps of the two-photon process occur under different excitation conditions. With regard to the orientation of the transition moment of the parent molecules, the first photon interacts with an isotropic molecular distribution, whereas the second photon encounters on orientated molecules due to the anisotropic selection of the first absorption process. Since any anisotropy can be destroyed by molecular motion, the influence of this effect may decrease when the delay time between the absorption steps becomes longer.

The precision of the deduced value of the second-photon absorption cross section is limited by possible shortcomings of the rate equation approach as a model for the two-photon excitation process as well as errors in the measurement itself. To check whether the various simplifications introduced in modeling the kinetics according to fig. 3 were justified, the system of coupled differential equations was solved numerically and found to lead to identical results compared to the calculation with the derived equations.

Possible measurement errors include the assumption that matching focal volumes are probed with well behaved Gaussian laser beams. Only then can the intensity be treated as spatially constant [24]. The geometrical conditions in our study, i.e. the focal volume and the overlap of the pump and probe lasers, have been investigated very accurately by applying the technique of velocity-aligned Doppler spectroscopy (VADS) [25] to the single-photon photolysis of H<sub>2</sub>O<sub>2</sub> at 266 nm [26,27]. In this case the beam sizes could be extracted as sensitive parameters in the fitting procedure of the VADS line shapes obtained at different delay times to the delay function. As the result of the VADS measurements it was confirmed that the dye laser beam completely envelops the photolysis focus and consequently, all of the spatially distributed emerging OH(X) radicals can be probed. Furthermore, any influence of spectrally narrowed detection due to the interference filter was excluded, since the (laser-induced) emission spectra following single-photon and two-photon excitation of H<sub>2</sub>O<sub>2</sub> at 266 nm were found to be very similar (vide infra). Corrections for minor contributing polarization effects, e.g. photofragment alignment, were not included. When all uncertainties are considered, a confidence range for  $\sigma_2$  of  $(1-5) \times 10^{-16}$  cm<sup>2</sup> is derived.

In addition to the determination at 266 nm,  $\sigma_2$  was measured at 193 nm by comparison with the total OH(A) fluorescence signal  $S''$  obtained from single-photon dissociation at 157 nm [11]. In the case of VUV excitation, one obtains for the volume normalized fluorescence signal:

$$S'' \propto [\text{OH(A)}]'' = [\text{H}_2\text{O}_2] \sigma'' Q'' I'' , \quad (9)$$

with  $\sigma'' = 1.5 \times 10^{-18}$  cm<sup>2</sup> and  $Q'' = 0.06$  [28] being respectively the absorption cross section and the quantum yield, at 157 nm. In our experiments irradiating 1.3 Pa H<sub>2</sub>O<sub>2</sub> with VUV laser light at an intensity of 66 mJ cm<sup>-2</sup> resulted in a fluorescence signal, which was about 70 times more intense than that following two-photon excitation at 193 nm with 4.4 J cm<sup>-2</sup>. The excitation volumes were identical and the energies have been corrected for the effect of preabsorption. Since the applied laser intensity at 193 nm efficiently saturated the A–X transition, eq. (4) has to be compared to eq. (3) which leads to

$$\sigma_2 = (S/S'') k_1 T \sigma'' Q'' (I''/I) . \quad (10)$$

The calculated differential second-photon absorption cross section  $\sigma_2 \approx 3 \times 10^{-18} \text{ cm}^2$  at 193 nm is approximately 60 times smaller than at 266 nm. This difference is definitely outside the error limits of both measurements and is taken as a clear indication that the quantum yield for OH(A) production decreases drastically with elevated photon energy as is expected due to dissociation via energetically favorable channels to non-fluorescing fragments [29]. The effect can also be seen in the single-photon excitation of  $\text{H}_2\text{O}_2$ , where the quantum yield of 0.18 at 130 nm drops sharply to  $<0.08$  at 106 nm [28]. Furthermore, the result indicates that the energetically possible decay into two OH(A) product radicals is extremely unlikely.

### 5. Internal state distribution

When nascent state distributions from photoinduced emission are investigated, the mean lifetime of the product radicals in the upper electronic state limits the useful experimental pressure range, since intermolecular processes can influence the total fluorescence intensity by quenching and the fragment state distribution by rovibrational relaxation processes. As long as quenching is substantially faster, the spectroscopic information is not spoiled by collisional relaxation. Differently to translationally excited OH( $X^2\Pi_i$ ) radicals, where rotational relaxation takes place at a gas kinetic rate [27,30], in the case of OH( $A^2\Sigma^+$ ) quenching with  $k_Q \approx 3 \times 10^{-10} \text{ cm}^3 \text{ molecule}^{-1} \text{ s}^{-1}$  [7,31] has been observed to be the faster process. This was experimentally confirmed, since the spectral structure did not show any pressure effects up to 7 Pa.

Fig. 4 shows the low-resolution emission spectra of OH( $A^2\Sigma^+$ ) following two-photon excitation of hydrogen peroxide at 193 nm (a) and 266 nm (b). The obvious vibrational bands are (1, 0) around 282 nm and (0, 0) + (1, 1) beyond 306 nm. From the integration of the single bands with correction for predissociation effects and normalization with regard to the vibrational transition probabilities [23] the relative yield at 193 nm for  $v' = 0$  to  $v' = 1$  was calculated to be 0.76:0.20. The determination of the population in  $v' = 2$  was complicated by strong predissociation and, therefore, is only estimated to be less than 0.04. At

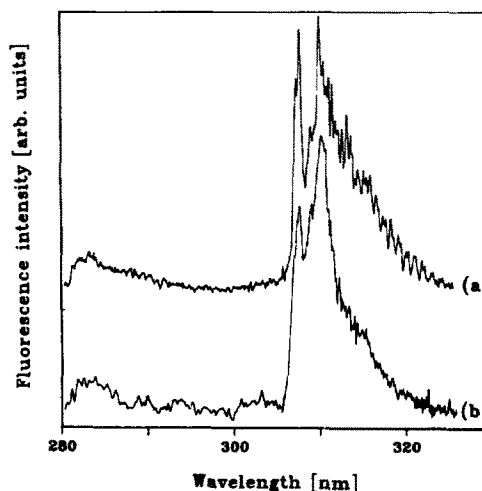


Fig. 4. Low-resolution fluorescence spectra of OH( $A^2\Sigma^+$ ) following two-photon excitation of hydrogen peroxide at 193 nm (a) and 266 nm (b). The vibrational bands to be seen are (1, 0) around 282 nm and (0, 0) + (1, 1) beyond 306 nm. Experimental conditions were 1.5 Pa (a) and 7.0 Pa (b) hydrogen peroxide irradiated at a laser fluence of  $50 \text{ MW cm}^{-2}$ .

266 nm we found 0.78:0.22 without  $v' = 2$  being detected. The corresponding vibrational partitioning in the 193 nm two-photon dissociation of deuterium peroxide was determined to be 0.63:0.27:0.10.

The rotational structure of the vibrational bands could not always be resolved, especially in the 266 nm experiment, where the low emission intensity did not allow exploitation of the full instrumental resolution. Therefore, at 266 nm no rotational state distribution in  $v' = 1$  can be given and only averages over all fine-structure components of a rotational transition were analyzed. As a dynamical feature of the photodissociation process of  $\text{H}_2\text{O}_2$  and  $\text{D}_2\text{O}_2$  at 193 nm the resolvable spin components were observed to be statistically populated. Our method of inverting overlapping rotational lines into population numbers by convolution of a simulated OH (OD) spectrum with the independently determined instrumental resolution and the subsequent least-squares fit procedure to the experimental spectrum has already been described [11].

Generally, fluorescence from electronically excited species generated by polarized photolysis is expected to be polarized, too. In the present study we diminished the influence of possibly existing polarization

effects due to product alignment by averaging over the lambda components of a rotational state.

From the population analysis we obtained the ro-vibrational distributions shown in fig. 5 for the OH( $A^2\Sigma^+$ ;  $v'=0$ ) vibrational state. When  $\ln[P(J')/2J'+1]$  is drawn as a function of the rotational energy in a Boltzmann plot, the observed rotational state distributions for two-photon dissociation can be described by straight lines with single rotational temperature parameters. For H<sub>2</sub>O<sub>2</sub> (D<sub>2</sub>O<sub>2</sub>) two-photon dissociation at 193 nm we found  $T_{v'=0}=3800\pm 100$  K ( $5170\pm 200$  K) and  $T_{v'=1}=4800\pm 100$  K ( $5100\pm 800$  K). At 266 nm a value of  $T_{v'=0}=2200\pm 150$  K resulted.

The total excess energy  $E_{av}$  for the two-photon dissociation process of R<sub>2</sub>O<sub>2</sub> (R=H, D) into two hydroxyl radicals at the wavelength  $\lambda$  is given by

$$E_{av} = 2hc/\lambda + E_{int}(R_2O_2) - D_0 - T_e, \quad (11)$$

with  $E_{int}(R_2O_2)$  being the internal energy of the parent molecule,  $D_0$  the dissociation energy [32], and  $T_e$  the term value for the OR( $A^2\Sigma^+$ ) state [33]. The internal energy  $E_{int}(R_2O_2)$  is mainly determined by the rotational energy of the parent ( $\approx 3.7$  kJ mol<sup>-1</sup>) and the vibrational energy of the  $\nu_4$  torsional mode ( $\leq 1.6$  kJ mol<sup>-1</sup>). The partitioning of the available energy calculated following eq. (11) into product ex-

citation is shown in table 1. The fractions of  $E_{av}$  released as vibration and rotation in the OR( $A^2\Sigma^+$ ) radical are:

$$f_{vib}(A) = \sum_{v'} P(v') E_{vib}(v') / E_{av}, \quad (12)$$

$$f_{rot}(A) = \sum_{N'} P(N') E_{rot}(N') / E_{av}. \quad (13)$$

Furthermore, the calculated maximum fraction of the available energy that can be transferred theoretically into OR translation is given by

$$f_{tr}^{max} \equiv f_{tr}^{max}(A) = f_{tr}^{max}(X) \\ = \frac{1}{2} [1 - f_{vib}(A) - f_{rot}(A)], \quad (14)$$

when one assumes OH(X) partner fragment formation without internal excitation. The fractions for OH(A) and OH(X) are identical due to conservation of linear momentum.

## 6. Two-photon dissociation dynamics

In fig. 5 the experimentally observed OH( $A^2\Sigma^+$ ;  $v'=0$ ) rotational energy distributions from two-photon dissociation of H<sub>2</sub>O<sub>2</sub> are contrasted with those following near-isoenergetic single-photon VUV excitation. The characteristic and obvious feature of the latter processes is very high rotational excitation of the OH(A) product. In the photolysis at 157 nm the partially inverted rotational state distribution peaks at  $N'_{OH} \approx 21$  with a very narrow width (fwhm) of  $\Delta N'_{OH} \approx 6$  [11]. The vibrational mode of the OH(A) fragments was only weakly excited. Expressed in terms of energy partitioning, more than 44% of the available energy is released in OH(A) rotation (see table 1). The rotational state distributions following dissociation at 147 and 124 nm show a similar structure with the population maximum at  $N'_{OH} = 21-22$  and a systematic broadening to  $\Delta N'_{OH} \approx 8$  and 11, respectively [16].

Interpretation of the energy disposal data leads to a model for the single-photon VUV dissociation of hydrogen peroxide, where the major part of fragment rotation is induced by a strong torsional dependence of the upper state potential. Conservation of energy and angular momentum together with the observed OH(A) alignment [11] demands that the simulta-

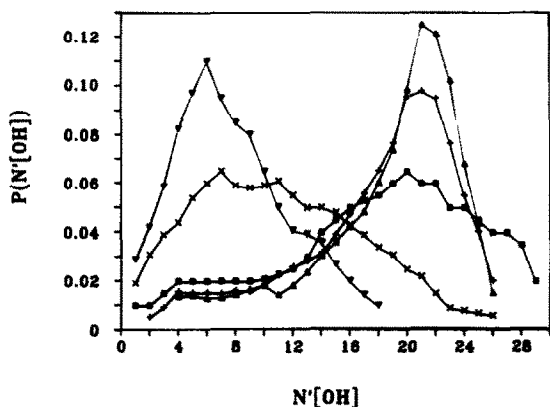


Fig. 5. Comprehensive view of OH( $A^2\Sigma^+$ ,  $v'=0$ ) rotational energy distributions from single-photon VUV dissociations of H<sub>2</sub>O<sub>2</sub> at 124 nm (■) [16], 147 nm (+) [16], and 157 nm (▲) [11] compared to the near-isoenergetic two-photon processes at 193 nm (×) and 266 nm (▼). Population numbers are corrected concerning predissociation and are normalized by  $\sum_{N'} P(N') = 1$ .



Table 1

Energy partitioning in  $\text{OH}(\text{A}^2\Sigma^+)$  from the dissociation of  $\text{R}_2\text{O}_2(\tilde{\text{X}}^1\text{A})$  into  $\text{OH}(\text{X}^2\Pi_1)$  and  $\text{OH}(\text{A}^2\Sigma^+)$  following resonant  $n$ -photon excitation at wavelength  $\lambda$  (nm). Energies are given in  $\text{kJ mol}^{-1}$ . Dissociation energies and term values used for the calculation of the available energy  $E_{\text{av}}$  are as follows:  $D_0(\text{H}_2\text{O}_2)=197 \text{ kJ mol}^{-1}$ ,  $D_0(\text{D}_2\text{O}_2)=204 \text{ kJ mol}^{-1}$  [32],  $T_e(\text{OH}[\text{A}])=388 \text{ kJ mol}^{-1}$ ,  $T_e(\text{OD}[\text{A}])=391 \text{ kJ mol}^{-1}$  [33]

R	$n$	$\lambda$	$E_{\text{av}}$	$E_{\text{vib}}(\text{A})$	$E_{\text{rot}}(\text{A})$	$f_{\text{vib}}(\text{A})$	$f_{\text{rot}}(\text{A})$	$f_{\text{tr}}^{\text{max}}$	Ref.
H	1	124	388		76		0.20		[16]
H	1	147	233		72		0.31		[16]
H	1	157	179	3.4	79	0.02	0.44	0.27	[11]
D	1	157	170	2.5	47	0.02	0.28	0.35	[11]
H	2	193	657	9.7	32	0.01	0.05	0.47	this work
D	2	193	648	13.1	42	0.02	0.06	0.46	this work
H	2	266	319	8.4	18	0.03	0.06	0.46	this work

neously formed  $\text{OH}(\text{X})$  partner fragment is also rotationally hot. Hence it follows that the kinetic energy of both fragments must be rather low (at 157 nm:  $v_{\text{OH}} \approx 1700 \text{ m s}^{-1}$  and  $v_{\text{OD}} \approx 1900 \text{ m s}^{-1}$ ). The identification of the torsional motion, which results predominantly from the strong dependence of the potential energy on the dihedral angle, as the promoting mode is supported by the ab initio calculations of Meier et al. [14]. There all suitable excited states show an energy gradient of several eV around the Franck–Condon region in that coordinate.

The  $\text{OH}(\text{A})$  rotational state distributions following two-photon excitation at 266 and 193 nm are drastically different than those following single-photon VUV dissociation, although the total energies available to the products are of the same magnitude. Surprisingly, the two-photon induced  $\text{OH}(\text{A})$  rotational state distribution at 266 nm resembles the distribution of  $\text{OH}(\text{X}^2\Pi_1)$  following single-photon dissociation at the same wavelength and thus half the photon energy rather than the distribution of the near-isoenergetic process at 124 nm. Photolysing  $\text{H}_2\text{O}_2$  with a single photon at 266 nm yields a Gaussian distribution of rotational states with the peak population at  $N''_{\text{OH}}=6$  and  $\Delta N''_{\text{OH}}=9$  [9]. At 193 nm the two-photon induced  $\text{OH}(\text{A})$  rotational state distribution is indeed twice as broad as the corresponding one-photon  $\text{OH}(\text{X})$  distribution ( $f_{\text{rot}}[\text{X}]=0.08$  for each hydroxyl radical [10]), but the fraction of available energy released in product rotation is nearly the same. Since the fragments from the two-photon dissociation possess a much lower internal energy than those following VUV photolysis at a compara-

ble photon energy, they must be generated with very high translational energy. From the values of  $f_{\text{tr}}^{\text{max}}$  calculated according to eq. (14) we obtain  $v_{\text{OH}}^{\text{max}} \approx 6000 \text{ m s}^{-1}$  and  $v_{\text{OD}}^{\text{max}} \approx 5700 \text{ m s}^{-1}$  for the 193 nm two-photon processes and  $v_{\text{OH}}^{\text{max}} \approx 4200 \text{ m s}^{-1}$  for the corresponding 266 nm excitation.

For energetic reasons the two-photon processes develop on the same final singlet states as the single-photon processes. Transitions to existing triplet states, possible in principle, require spin inversion and are excluded due to the expected low transition probability. In the two-photon dissociation of hydrogen peroxide the second-photon absorption is found to be more probable than the first step by a factor of  $\sigma_2/\sigma_1 \approx 5000$ . However, from comparison of the efficiencies of  $\text{OH}(\text{A})$  formation in the single-photon and two-photon processes one may calculate the overall cross section  $\sigma_{12}$  for the two-photon dissociation as the geometrical average over both individual cross sections. At 266 nm a value of  $\sigma_{12} \equiv (\sigma_1\sigma_2)^{1/2} \approx 3 \times 10^{-18} \text{ cm}^2$  results. The fluorescence cross section for the single photon excitation at 133 nm is  $\sigma \approx 1.3 \times 10^{-18} \text{ cm}^2$  [28]. Thus, both isoenergetic excitation pathways have approximately the same  $\text{OH}(\text{A})$  yield.

Since different upper electronic molecular states cannot be responsible for the experimentally observed dynamical distinction, it is obvious that the trajectories of the two-photon process on the final repulsive potential surface must be different from those for single-photon excitation. The drastically lowered fragment rotation implies a dynamical picture where the evolution of the intermediate state removes the molecular system away from the Franck–Condon re-

gion within the delay time  $\tau$  (see fig. 1). Then absorption of the second photon proceeding from a molecular structure which differs essentially from that of the ground state ( $\chi \approx 120^\circ$ ) with presumably a trans-planar conformation ( $\chi \approx 180^\circ$ ), causes transition into a region on the final potential energy surface which is nearly flat with regard to the dihedral angle  $\chi$ . This transition to the final state occurs predominantly at large O–O internuclear separations, since within the lifetime of the intermediate state  $\tau$  both accelerated OH fragments are substantially displaced from the equilibrium distance. At 266 nm the separation attains about 75% of the initial O–O bond length based on a simple kinematic model [21]. Consequently, only a small rotational excitation is added by the torsional dependence of the upper state potential to the angular momentum gained in the first absorption step.

A fascinating experiment would be the application of time-variable femtosecond laser pulses to the two-photon excitation of hydrogen peroxide, where we would expect to observe a continual convergence of the Boltzmannian rotational state distribution induced by two-photon excitation into the inverted distribution following isoenergetic single-photon dissociation either by gradually shortening the excitation pulse or by diminishing the delay time between colliding pulses in a dual beam experiment. However, interference phenomena [20] have to be considered. A laser delivering nanosecond or picosecond pulses operates in a quasi-cw regime, where the wave packet is built out of a convolution of outgoing waves, as long as population remains in the ground state. Differently, for a true femtosecond system there is a single outgoing pulse.

### Acknowledgement

This work has been performed as part of a program of the Deutsche Forschungsgemeinschaft (DFG), whose financial support is gratefully acknowledged. We thank R. Fasold for her assistance in some part of the experimental work. Highly concentrated hydrogen peroxide was kindly supplied by DEGUSSA.

### References

- [1] B. Honig, J. Jortner and A. Szöke, *J. Chem. Phys.* 46 (1967) 2714.
- [2] R.J. Donovan, in: *Specialist Periodical Report, Vol. 4. Gas Kinetics and Energy Transfer*, eds. P.G. Ashmore and R.J. Donovan (Chem. Soc., London, 1981).
- [3] S. Kimel and S. Speiser, *Chem. Rev.* 77 (1977) 437.
- [4] N. Shafizadeh, J. Rostas, J.L. Lemaire and F. Rostas, *Chem. Phys. Letters* 152 (1988) 75;  
C.G. Atkins, R.G. Briggs, J.B. Halpern and G. Hancock, *Chem. Phys. Letters* 152 (1988) 81;  
R.G. Briggs, J.B. Halpern, G. Hancock, N. Shafizadeh, J. Rostas, J.L. Lemaire and F. Rostas, *Chem. Phys. Letters* 156 (1989) 363.
- [5] L. Bigio, R.S. Tapper and E.R. Grant, *J. Phys. Chem.* 88 (1984) 1271, 1273;  
L. Bigio and E.R. Grant, *J. Chem. Phys.* 83 (1985) 5361; 87 (1987) 360;  
L. Bigio, G.S. Ezra and E.R. Grant, *J. Chem. Phys.* 83 (1985) 5369.
- [6] P.H. Cribb and J. Brickmann, *Ber. Bunsenges. Physik. Chem.* 90 (1986) 162.
- [7] C.B. McKendrick, E.A. Kerr and J.P.T. Wilkinson, *J. Phys. Chem.* 88 (1984) 3932.
- [8] H. Gölsenleuchter, K.-H. Gericke and F.J. Comes, *Chem. Phys. Letters* 116 (1985) 61.
- [9] K.-H. Gericke, S. Klee, F.J. Comes and R.N. Dixon, *J. Chem. Phys.* 85 (1986) 4463;  
S. Klee, K.-H. Gericke and F.J. Comes, *Ber. Bunsenges. Physik. Chem.* 92 (1988) 429.
- [10] A.U. Grunewald, K.-H. Gericke and F.J. Comes, *Chem. Phys. Letters* 132 (1986) 121; *J. Chem. Phys.* 87 (1987) 5709;  
A. Jacobs, M. Wahl, R. Weller and J. Wolfrum, *Appl. Phys. B* 42 (1987) 173.
- [11] H. Gölsenleuchter, K.-H. Gericke, F.J. Comes and P.F. Linde, *Chem. Phys.* 89 (1984) 93;  
K.-H. Gericke, H. Gölsenleuchter and F.J. Comes, *Chem. Phys.* 127 (1988) 399.
- [12] E.M. Evleth, *J. Am. Chem. Soc.* 98 (1976) 1637;  
C. Chevaldonnet, H. Cardy and A. Dargelos, *Chem. Phys.* 102 (1986) 55.
- [13] E.A. Reinsch, *Chem. Phys. Letters* 141 (1987) 369.
- [14] U. Mcier, V. Stacmmler and J. Wasilewski, to be published.
- [15] U. Gerlach-Meyer, E. Linnebach, K. Kleinermanns and J. Wolfrum, *Chem. Phys. Letters* 133 (1987) 113.
- [16] K.H. Becker, W. Groth and D. Kley, *Z. Naturforsch.* 20a (1965) 748;  
H. Okabe, *J. Chem. Phys.* 72 (1980) 6642.
- [17] P.A. Giguere and P. Geoffrion, *Can. J. Res. B* 27 (1949) 168.
- [18] J.P. Simons, A.J. Smith and R.N. Dixon, *J. Chem. Soc. Faraday Trans. 2* 80 (1984) 1489.
- [19] M.L. Sink, A.D. Bandrank and K. Lefebvre, *J. Chem. Phys.* 73 (1980) 4451.

- [20] S.O. Williams and D.G. Imre, *J. Phys. Chem.* 92 (1988) 3363, 6636.
- [21] S. Klee, K.-H. Gericke and F.J. Comes, *J. Chem. Phys.* 85 (1986) 40.
- [22] L.T. Molina and M.J. Molina, *J. Photochem.* 15 (1981) 97.
- [23] W.L. Dimpfl and J.L. Kinsey, *J. Quant. Spectry. Radiative Transfer* 21 (1979) 233.
- [24] D.R. Crosley and G.P. Smith, *J. Chem. Phys.* 79 (1983) 4764.
- [25] Z. Xu, B. Koplitz and C. Wittig, *J. Chem. Phys.* 90 (1989) 2692.
- [26] R.N. Dixon, J. Nightingale, C.M. Western and X. Yang, *Chem. Phys. Letters* 151 (1988) 328.
- [27] S. Klee, K.-H. Gericke and F.J. Comes, to be published.
- [28] M. Suto and L.C. Lee, *Chem. Phys. Letters* 98 (1983) 152.
- [29] L.J. Stief and V.J. DeCarlo, *J. Chem. Phys.* 50 (1969) 1234.
- [30] A.U. Grunewald, Dissertation, University Frankfurt am Main, FRG (1989).
- [31] K.-H. Gericke, R. Klinke and F.J. Comes, to be published.
- [32] K.-H. Gericke, A.U. Grunewald, S. Klee and F.J. Comes, *J. Chem. Phys.* 88 (1988) 6255.
- [33] K.P. Huber and G. Herzberg, in: *Molecular Spectra and Molecular Structure*, Vol. 4. Constants of Diatomic Molecules (Van Nostrand, Princeton, 1979) pp. 508, 514.